

Conf CONE-900822--33
DE92 004290

(contributed to: XXVth Int. Conf. on High Energy Physics, Singapore, Aug. 2-8 1990)

MEASUREMENT OF THE J/Ψ ELASTIC PHOTOPRODUCTION
FROM 100 GEV TO 400 GEV IN THE EXPERIMENT E687 AT FERMILAB

P.L. Frabetti

Dipart. di Fisica dell'Università and Sezione INFN, via Irnerio, 42, Bologna, Italy
C.W. Bogart, P. Caneva¹, S. Culy, J.P. Cumalat, D. Kaplan²

Department of Physics, University of Colorado, Boulder, Colorado, USA

J. Butler, E. Daviport³, H. Gaines, P. Garbincius, S. Gourlay,
D. Harding, P. Kasper, A. Kreymer, P. Letourneau, H. Mendez⁴

Fermilab, P.O. Box 5000, Batavia, Illinois 60510, USA

S. Bianco, M. Giorini, F.L. Fabbri, A. Spallone, A. Zilio

Laboratori Nazionali di Frascati dell'INFN, via E. Fermi, 2, Frascati, Italy

R. Chubertson, M. Diesburg⁵, J. Jaross, K. Lingel, J.R. Wilson, J.E. Wiss

Department of Physics, University of Illinois, Urbana, Illinois, USA

G Bellini, M. Di Corato, M. Giannarchi, P. Inzani, S. Malvezzi, P.E. Manfredi⁶,

D. Menasce, L. Moroni, D. Pedrini, L. Perasso, A. Sala, S. Sala, D. Torretta, M. Viitome⁷

Dipartimento di Fisica dell'Università and Sezione INFN, via Celoria, 16, Milano, Italy
D. Buchholz, C. Castoldi⁸, B. Gobbi, S. Park, R. Yoshida

Dept of Physics and Astronomy, Northwestern University, Evanston, Illinois, USA

J.M. Bistagni, J.K. Busenitz⁹, N.M. Cason, R.W. Gardner, C.J. Kennedy, E.J. Manni,
R.J. Mountain, D.L. Pusey, R.C. Ruchti, W.D. Shepherd, M.G. Zambrano

Department of Physics, University of Notre Dame, Notre Dame, IN 46556, USA
G.L. Bocca, R. Di Stefano, S.P. Ratti, P. Vitiello

Dipartimento di Fisica Nucleare e Teorica dell'Università and Sezione INFN,
via A. Bassi, 6, Pavia, Italy
A. Lopez

Physics Department, University of Puerto Rico at Mayaguez, Puerto Rico
(presented for the E687 Collaboration by S.P. Ratti)

Acc 2 - 76ER02289

1- Present address: HERA TII Watson Laboratories, Yorktown Heights, NY 10598 (USA)

2- Present address: University of Oklahoma, Norman, OK 73019 (USA)

3- Present address: University of North Carolina, Asheville, NC (USA)

4- Also: CIINVESTAV-IPN, A.P. 14740, 07080 Mexico D.F., Mexico

5- Present address: Fermilab, Batavia, IL 60510 (USA)

6- Present address: Dipartimento di Elettronica dell'Università, Pavia (Italy)

7- On leave from Istituto Nazionale di Fisica Nucleare, Sezione di Pavia, Pavia (Italy)

8- Present address: University of Alabama, University, AL 35486 (USA)

*- Supported in part by Ministero della Università e della Ricerca Scientifica

CONFIDENTIAL
DO NOT COPY

1. Introduction

The Fermilab experiment E687 used the Wide Band Photon Beam with the endpoint photon energy off about 4500 GeV to study production and decay of charmed particles at the highest energy off a photon beam made available at present by accelerators/^{1a}.

Among the different trigger setups to select charm candidates, a multimuon trigger enabled us to select a sample off J/ψ particles decaying into muon pairs and to measure the cross section for elastic J/ψ photoproduction on a Be target at previously unattained photon energies, as high as about 4000 GeV.

Photoproduction off J/ψ has been observed at Fermilab, Slac and Cornell, immediately after the discovery of the J/ψ in 1974; elastic photoproduction off J/ψ has been measured from some 100 GeV to about 2500 GeV by several authors/^{2a}, both on nuclei and on hydrogen. Photoproduction, at that time, was interpreted in terms of the Vector Meson Dominance (VMD) Model proposed by J.I. Sakurai/^{3a} to describe the photoproduction of low mass vector mesons as due to the vector meson component off the hadronic structure of the photon. The Model was found to be very satisfactory/^{3b}; in particular, combined with the Additive Quark Model (AQM), it shows impressive agreement with the $d\sigma/dt$ differential cross section for ρ photoproduction and good agreement to the ω and ϕ data/^{3b}.

The more recent Photon Gluon Fusion (PGF) Model inspired by QCD/^{4a} seems to provide a better description of the J/ψ data due to the relatively large mass of the charmed quark that makes it possible to perform perturbative QCD calculations and thus to make definite predictions on the energy dependence of the J/ψ photoproduction cross section.

The two basic processes are sketched and compared in fig. 1. The VMD Model assumes that the direct coupling off the photon to the vector meson dominates the process, the remaining interaction being just the scattering off the vector meson off the target nucleon (fig. 1a). The PGF Model, on the other hand, is based on the cross section calculation from the elementary process off fig. 1b. Such process is closely related to the Bethe Heitler QED process/^{5a} generating a $\mu^+\mu^-$ pair in the nuclear field off the target.

In 1985, Holness, Lee and Wiss published an extensive compilation of experimental data/^{2a} to which the data from the Cern NA14 experiment/^{2b} has to be added.

In the present paper we give the experimental measurement off the cross section per nucleon for the elastic J/ψ photoproduction in six energy intervals from 1000 GeV to 4500 GeV; the overall $d\sigma/dt$ differential cross section, as well as an estimate off the coherent diffractive photoproduction off the Be nucleus. We will finally compare the energy dependence off our measured cross sections with the predictions off the PGF Model.

2. Beam setup and apparatus

The beam setup and the apparatus used to detect the elastic J/ψ photoproduction as well as the final states containing heavy flavours such as charm, and possibly bottom, are described elsewhere/^{6a}. Here we very briefly recall the points relevant to the present measurement: i.e. some features of the beam and of the muon detector/trigger.

2.1 Beam

The Wide Band Photon Beam^[6a] is a "bremsstrahlung beam". The 850 GeV protons strike a 45.7 cm Be upstream target; charged particles are swept away to produce a neutral beam (48% neutron, 48% photons, 2% K^0 plus others). The neutral beam impinges on a 0.3 radiation lengths Pb converter, to produce electron-positron pairs. From the converter, the electron component (off energy E_e) is magnetically separated and transported to a second radiating Pb foil (0.3 radiation lengths) which finally produces via bremsstrahlung a photon beam whose momentum bite is essentially defined by the acceptance of the electron transport line ($\pm 15\%$ of the central setting off the electron beam). A set of counters immediately after the radiator, measures the energy E_γ of the scattered electron after bremsstrahlung to give an estimate off the photon energy $E_\gamma = E_0 \cdot E_\gamma$.

The bremsstrahlung beam has the advantage of containing a negligible neutral hadron background. Since the interaction lengths of both converter and radiator are small, the resulting neutron contamination turns out to be $\sim 10^{-5}$ per photon from MonteCarlo simulation.

From an initial beam off typically 10^{12} protons per 20 sec spill, the electron beam line transports about 2×10^7 electrons giving rise to 10^7 photons and approximately 10^{41} photons producing hadrons in our 10% interaction length Be target.

2.2 Apparatus

The apparatus^[6b] (fig. 2) is made off a Be target, a high resolution 12 planes microstrip silicon detector's spectrometer, a proper set off trigger and veto counter's hodoscopes, two large aperture magnets, a five multiwire proportional chamber's tracking system, three Cherenkov gas counters, two hadronic and two electromagnetic calorimeters, two muon detectors. The electro-magnetic calorimeters and muon detectors are split into an inner part (± 30 mrad) and an outer part (± 30 to ± 100 mrad) to provide proper angular coverage. The hadron calorimeter has a small central part (CHC) to cover the beam hole that exists all along the spectrometer. At the end of the detector, in front of the CHC and the inner muon detector, a Beam Gamma Monitor (BGM) is located; very little material exists between this location and the target. It covers ± 4 mrad and it is made of 45 Pb layers, 0.32 cm thick, interleaved with 1 cm thick lucite.

Relevant to this paper are the BGM, used to directly measure the total number of photons transported to the target and the muon system, used in the second level trigger.

For the purpose of the present paper only the inner muon detector has been used to trigger and to select/detect the muons from the decay off the J/ψ . The inner muon system is made of three planes of scintillators and four planes of proportional tubes, organized in both horizontal and vertical setups, covering ± 30 mrad.

A Master Gate (MG) rejects the copious electromagnetic gamma conversion into electron-positron pairs by detecting at least a large angle particle, some 20 m downstream off the target; it also vetoes on the muon halo escaping the charged particles beam dump absorbers in the beam line. The second level trigger requires at least 30 GeV in the hadron calorimeter or at least two muons.

3. Data analysis and differential $dN/d(-t)$ distribution

In this section we present the selection of our inelastic and elastic J/ψ sample and the fit of the $-t$ differential distribution to exponential curves, to extract both the nuclear elastic and the coherent component.

3.1 Selection of the J/ψ sample

Approximately 6×10^7 events were written on tape during the period December 1987-March 1988. The events for the present analysis were first selected according to the following criteria:

- 1- second level trigger equal two muons;
- 2- only two tracks of opposite sign verticalizing in the target;
- 3- at least one track identified as muon;
- 4- invariant mass of the dimuon larger than 1.0 GeV.

These criteria produced 2300 candidates whose invariant mass distribution is shown in fig. 3. A clear signal of the J/ψ can be seen at the right mass location with very little background at this stage. Due to the narrow width of the J/ψ particle, the peak is very close to a gaussian; a fit to the invariant mass distribution for $m > 2.5$ GeV gave a mass value $M = (3.094 \pm 0.006)$ and a width $\sigma = (0.06 \pm 0.05)$ in good agreement with the values reported in the Particle Data Book [7].

The elastic events have been selected on the basis of a cut $\Delta M/\sigma < 3$ and on the basis of energy. Fig. 4a shows the difference between the measured energy of the photon and the measured energy of the dimuons from the J/ψ decay; fig. 4b shows the invariant mass of the selected sample of elastic J/ψ 's.

Due to the vector nature of the J/ψ , coherent diffractive photoproduction off the Be nucleus is possible which should appear in the four-momentum transfer squared, $-t$ distribution as a steep $\exp(-gt)$ component at very small t . Values around $g=40$ have been obtained in several photoproduction experiments on heavy nuclei [2b, 2h, 8]. In order to measure the photoproduction cross section per nucleon, the coherent part has to be subtracted.

3.2 Four-momentum transfer squared distribution

The $dN/d(-t)$ distribution of the elastic sample for all energies is shown in fig. 5. The background from the Bethe-Heitler process (outside the region of the J/ψ mass) is very well below 0.002 GeV $^{-2}$ and it might contaminate slightly only the first bin.

The distribution has been fitted sequentially to two exponential forms. Coherent production doesn't survive values of $-t > 0.15$ GeV 2 ; therefore, the distribution for $-t > 0.15$ GeV 2 has been fitted to the form:

$$\frac{dN}{d(-t)} = A e^{[-a(-t) + b(-t)^2]} \quad (1)$$

The values $A=615$; $a=4$; $b=1.5$ were obtained with a χ^2 value over degrees of freedom of 0.97. The fitted curve is shown as a full line in fig. 5.

Fixing the above values, a fit to the whole distribution was performed with the formula:

$$\frac{dN}{d(-t)} = \frac{dN^{\text{co}}}{d(-t)} + Be^{-g|t|} \quad (2)$$

The values $B=2100$ and $g=30$ were obtained with a χ^2 value over degrees of freedom of 0.56. The fitted curve is shown as dashed line in fig. 5.

The goodness of the fit indicates that the Bethe-Heitler background is indeed very low (excluding the first point would not change the values of the fitted parameters). The coherent term in formula (2) accounts for (70 ± 2.7) events, where the error is estimated from the covariant matrix of the fit. The estimate for the coherent cross section will be done in the next section.

4. Elastic cross section measurement

There are two basic methods to measure the J/ψ elastic photoproduction cross section/ ρ . One can rely directly on the measurement of the integrated flux of incident electrons (measured in a special run with the final Pb radiator out of the beam and the sweeping magnets off so that the electrons were transported directly to the BGMI calorimeter); the BGMI counts where the signal is discriminated at the level where the energy deposited corresponds to 133 GeV or more, the effective length of the target accounting for the actual targeting efficiency ($\epsilon_t = 54.35\%$), the estimated correction for the availability of the second level trigger after MG and the known branching ratio $BR_{J/\psi \rightarrow \mu\mu}$.

In such a case the cross section per nucleus can be written as:

$$\sigma_{J/\psi} = \frac{N_{J/\psi}}{A_{J/\psi} N_t N_A \rho d \epsilon_t L BR_{J/\psi \rightarrow \mu\mu}} \quad (3)$$

where:

$N_{J/\psi}$ is the number of detected J/ψ ;

$A_{J/\psi}$ is the acceptance -including master gate trigger, reconstruction, track linking, vertex finding, invariant mass cuts etc.- calculated by proper MonteCarlo simulations;

ρ is the target density;

d the target length;

ϵ_t the targeting efficiency determined by the beam profile and the target geometry;

L the corrective factor determined by the fraction of gated MG triggers to the ungated MG triggers;

N_A the total number of nuclei per unit area;

N_γ the total number of incoming photons obtained by the BGMI counts corrected for the shape of the photon spectrum;

BR the branching ratio for $J/\psi \rightarrow \mu\mu$.

Alternatively one can rely upon the normalization to the Bethe Heitler dimuon production, a well known and calculable QED process which appears as background off the J/ψ signal. In this way, all target factors as well as the factor L , cancel out since both types of events are recorded in the same experimental conditions; many other systematic errors also cancell out.

In such a case the cross section per nucleon is simply:

$$\sigma_{J/\psi} = \frac{N_{J/\psi} A_{BH} \sigma_{BH}}{N_{BH} A_{J/\psi} BR_{J/\psi \rightarrow \mu\mu}} \quad (4)$$

where:

σ_{BH} is the cross section for the dimuon Bethe-Heitler production per nucleon;

N_{BH} is the number of Bethe-Heitler dimuons;

$A_{J/\psi}$ is the acceptance for the J/ψ particles;

A_{BH} the acceptance of the Bethe-Heitler dimuons;

BR the branching ratio for $J/\psi \rightarrow \mu\mu$.

The values of A_{BH} and σ_{BH} are obtained by a proper MonteCarlo simulation of the Bethe-Heitler process and the incoming number of photons can be calculated from the number of Bethe-Heitler dimuons.

The available energy range above 100 GeV, has been subdivided into six energy intervals for the purpose of measuring the elastic J/ψ photoproduction cross section.

Fig. 6a shows the comparison between the photon spectrum from the BGM count rates and the spectrum calculated from Bethe-Heitler dimuons. The agreement between the two methods is very good. The region below 100 GeV (not used, see fig. 7 below) is also shown. Fig. 6b shows the complete spectrum obtained by MonteCarlo simulation from the known electron beam spectrum.

In this paper we will follow the second method which is more bias free and verify the results using the first method on a sample independently selected from among "good" beam spills kept well under control.

Acceptance and reconstruction efficiencies were calculated using a spectrometer simulation in the framework of Geant/10/ which is a general detector simulation program. Elastic vector meson were generated/9b/ with an exponential $d\sigma/dt = A \exp(b(t-t_{\min}))$ with $b=4.0$ (no significant changes in acceptance are detected varying b from -1.0 to -4.0) and a $(1+\cos^2)$ decay distribution for the J/ψ . Bethe-Heitler dimuons were simulated/9a/ on the basis of the matrix elements of ref. 5. Faked data tapes were processed through the program chain used for real data. For J/ψ analysis the reconstruction and vertexing efficiencies were typically above 98%, with most of the corrections coming from acceptance. The acceptances, corrected for the efficiency of the detectors and the various algorithms are compared, for the two processes in fig. 7. The sharp drop off of the acceptance at low energies is due to the outer muon detectors not being used.

For E_γ larger than 100 GeV, both the elastic sample used in the previous section and the Bethe-Heitler events, have been split into energy bins of 50 GeV, the energy of the two muons being assumed to be the photon energy. Bethe-Heitler events with $-t > 0.05$ GeV^2 were cut to eliminate inelastic production not simulated by the MonteCarlo.

The number of events thus selected are shown in columns 3 and 4 of Table I. In column 2 the value of the photon energy, averaged over the photon spectrum is also given.

The calculated cross sections per nucleon are given in col. 5 of Table I where both statistical and systematic errors are given (the systematic errors mainly come from the subtraction of the coherent contribution).

The cross section's values are reported in fig. 8a.

By integrating over the photon energy range, the cross section for coherent photoproduction of J/ψ off Be nuclei turns out to be $\sigma_{\text{coher.}} = (28 \pm 11)$ nb.

The above measurements have been checked by directly measuring or using formula (3) on a sample of events selected in a somewhat more stringent way as to guarantee the proper calculation of the normalization parameters.

The new selection criteria were:

1- second level trigger equal two muons;

2- events coming from only a part of the Be target/6b,9b/;

- 3- events coming from "good spill" only/2b/;
 4- both muons linked in the microstrip spectrometer;
 5- dimuon invariant mass within 3 standard deviation from the J/ψ mass leading to 124 events in the peak having $\rightarrow 0.02 \text{ GeV}^2$ to cut the Bethe-Heitler background.

Application of formula (3) to these events split into the same six photon energy bins gave the values of the cross section reported in column 4 of Table II. In Table II coll. 6, the corresponding cross sections per nucleon, corrected by a factor $/8/A^{0.94}$ are repeated for a direct comparison. Conversely the cross section per nucleus of the Bethe-Heitler method are reported in coll. 3 of Table II. The values of the cross sections measured by the two method are well within the errors and indicate that they cannot be distorted by very large systematic effects. The cross sections directly measured are also reported in fig. 8a.

5. Comparison with previous results and with the PGF Model

In fig. 8b our measured cross sections per nucleon are compared to similar measurements found in the literature/2/. The cross section seems to steadily increase and stabilize around 20 nb above 200 GeV. Our data are important to establish that the cross section does not increase rapidly with increasing photon energy. The solid line drawn in fig. 8b is the prediction of the energy variation of the elastic photoproduction cross section of the J/ψ particle given by the Photon Gluon Fusion Model/4a/. The cross section is given by:

$$\sigma_{\gamma \rightarrow \infty}(M^2) = \frac{64\pi\alpha_m}{9M^2} \left\{ \left(1 + \frac{4m_c^2}{M^2} \frac{8m_c^4}{M^4} \right) \ln \left[\frac{M^2}{2m_c^2} \left(1 + \sqrt{1 - \frac{4m_c^2}{M^2} \frac{2m_c^2}{M^2}} \right) \right] \left(1 + \frac{4m_c^2}{M^2} \right) \sqrt{1 - \frac{4m_c^2}{M^2}} \right\} \quad (5)$$

where α is the electromagnetic and α_s is the strong coupling constant (assumed to be $\alpha_s=0.3$) at the charm mass scale, M the total energy in the photon-gluon CMS and m_c the mass of the c quark. The elementary cross section of formula (5) must be convoluted with the gluon momentum distribution $G(x)$ which has been assumed to be/4b/:

$$xG(x)=3(1-x)^5. \quad (6)$$

The cross section for the charmonium production is simply the integration of the convolution of the PGF cross section from the mass of the two c quarks to the mass of 2 D mesons/4b/, i.e.

$$\sigma_{\gamma N \rightarrow J/\psi N} = f \int_{4m_c^2}^{4m_D^2} \sigma_{\gamma \rightarrow \infty}(M^2) G\left(\frac{M^2}{s}\right) \frac{dM^2}{s} \quad (7)$$

The factor f in front of the integral is simply the branching fraction for the production of J/ψ rather than any other charmonium state, usually taken to be 1/7 under the assumption that the final states are equally divided among the accessible charmonium states/11/ (such assumption is contradicted by the experimental data on the photoproduction of ψ' which accounts only for 20% of the J/ψ /2a,2h/, but this doesn't affect the energy behaviour of the cross section). It may be pointed out that

$G(x)$ enter into (5) without being multiplied by an extra distribution function as it is the case for badroproduction.

Formula (5) depends upon the value of the mass assumed for the c quark. The PGF Model prediction using (6) and $m_c=1.5$ GeV is shown in fig. 8b as a solid line. The dotted line, also shown in fig. 8b is the prediction based on the gluon distribution function parametrized from measurements by a neutrino experiment and evolved to the momentum transfer of 10 GeV^2 using the Altarelli-Parisi equations/[2a]/[this is the so called "EHLQ" function]; such gluon distribution function is in reasonable agreement with experimental measurements at four momentum transfer squared/[2b]/ of 10 GeV^2 .

The scale of the cross section calculated with the PGF Model is not stable for small changes in the mass of the c quark. In order to check the stability of the predictions against variations of the quark mass and of the shape of the gluon momentum distribution function, in fig. 8c the same data of fig. 8b are compared to curves recalculated assuming different parameter values. The two curves of fig. 8b would be barely distinguishable in logarithmic scale; therefore only the full line is repeated in fig. 8c. The dashed line is obtained by using a gluon distribution function:

$$x \cdot G(x) = 0.15 (1-x)^7 \quad (8)$$

instead of function (6) and using $m_c=1.5$ GeV. The dashed dotted line, instead, is the prediction using (8) and $m_c=1.6$ GeV.

Clearly the predictions are very sensitive to the c quark mass. Nonetheless the trend of the data on elastic photoproduction cross sections with increasing energy is well reproduced also quantitatively when the somewhat arbitrary semilocal duality factor 1/7 mentioned above/[11]/ is introduced and $m_c=1.6$ GeV.

6.. Conclusions

In the present paper we have performed a series of measurements of J/ψ photoproduction on Berillium at the highest photon energies made available by existing accelerators.

In the range 100-400 GeV incident photon energy, we estimated the coherent production cross section of J/ψ off Be nuclei to be $\sigma=(28\pm11)\mu\text{b}$ and the slope of the four momentum transfer squared distribution $dN/d(-t)$ for elastic J/ψ production to be exponential of the type (1) with parameters $a=4.0$ and $b=1.5$.

The elastic cross section has been measured in six photon energy intervals in the range 100-450 GeV, normalizing the event rate to the Bethe-Heitler dimuon production cross section, thus extending by 200 GeV the energy in which photoproduction of the J/ψ particle has been experimentally investigated. The measurements have been also performed by normalizing the event rate to a direct beam counting. The measured cross sections display little variation with increasing energy and the trend is in agreement with the predictions of the Photon-Gluon Fusion Model.

By the time of the Conference a further refinement of the analysis might be available.

7. Acknowledgments

We acknowledge the contributions of the technical staff of Fermilab - the Physics Department, the Research Division, the Computer Division, operators and DAQ group, the Accelerator Division- the Physics Departments of the participating Institutions, and INFN of Italy for their restless application to the recovery of the experimental apparatus after the fire that took place in the Wide Band Beam Laboratory on October 2nd 1987. They all made the present experiment possible.
 This research was supported in part by the National Science Foundation, the U.S. Department of Energy, the Italian Istituto Nazionale di Fisica Nucleare and Ministero della Università e della Ricerca Scientifica.

TABLE I: ELASTIC J/ψ PHOTOPRODUCTION CROSS SECTIONS (nb/nucleon)

ΔE	E_{av}	EVENTS		CROSS SECTION	
		Bethe-Heitler	J/ψ	Bethe-Heitler	Direct Meas. A ^{0.94} factor
100-150	121	327	43	13.4±(3.3±1.3)	9.4±2.5
150-200	177	238	65	18.0±(4.1±1.8)	15.7±3.4
200-250	223	156	55	15.2±(3.7±1.5)	14.5±3.5
250-300	272	96	65	19.4±(4.6±1.9)	16.4±4.1
300-350	324	48	52	29.0±(7.9±2.9)	24.3±6.4
350-450	374	10	11	21.6±(11.8±2.2)	17.9±9.5

TABLE II: ELASTIC J/ψ PHOTOPRODUCTION CROSS SECTION (nb/nucleus)

ΔE	E_{av}	Bethe-Heitler A ^{0.94} factor		Direct Meas. on Be
		$\sigma(nb)$	$\sigma(nb)$	
100-150	121	105.5±(26.1±10.3)		73.4±21.7
150-200	177	142.1±(32.4±14.2)		123.8±27.2
200-250	223	120.0±(29.2±11.8)		114.4±27.8
250-300	272	153.3±(36.3±15.0)		129.9±32.1
300-350	324	229.0±(62.3±22.9)		191.9±50.5
350-450	374	170.6±(93.2±17.4)		141.4±74.8

8. References

1. M. Binkley et al., "High Energy Photoproduction of States Containing Heavy Quarks and Other Rare Phenomena". Proposal in "Current Experiments in Elementary Particle Physics" Ed. by C.G. Wohl et al., LBL Report LBL-91 revised (Sept. 1989);
- 2a. S.T. Holmes, W. Lee, J.E. Wiss, Ann Rev Nucl Part Sci. **35**, 397 (1985);
- 2b. B. Knapp et al., Phys Rev Lett. **34**, 1040 (1975);
- 2c. U. Camerini et al., Phys Rev Lett. **35**, 483 (1975);
- 2d. B. Gittelman et al., Phys Rev Lett. **35**, 1616 (1975);
- 2e. T. Nasir et al., Phys Rev Lett. **36**, 1233 (1976);
- 2f. M. Binkley et al., Phys Rev Lett. **48**, 73 (1978); **50**, 302 (1983);
- 2g. R.H. Dentry et al., Phys Rev Lett. **52**, 795 (1984);
- 2h. R. Barate et al., Z Phys C Part and Fields. **33**, 505 (1987);
- 3a. J.I. Sakurai, Ann. Phys. **33**, 1 (1960);
- 3b. T.H. Bauer et al., Rev Mod Phys. **51**, 261 (1974);
- 4a. L.M. Jones and H.W. Wyld, Phys Rev. **D17**, 759 (1978);
- 4b. M. Gluck and E. Reya, Phys Lett. **79B**, 453 (1978);
- 4c. E.L. Berger and D. Jones, Phys Rev. **D23**, 1521 (1981); Phys Lett. **121B**, 61 (1983);
5. See e.g. Y.S. Tsai, Rev Mod Phys. **46**, 815 (1974);
- 6a. J. Butler et al. "Design for a New Wide band Neutral Beam for the Tevatron"; Fermilab Library TM-963 6020.000 (1980)
- 6b. S. Courlay et al., "Description of the E687 Spectrometer"; Report FN-553 1990 Data Particle Group, Phys Lett. **B204**, 1 (1988);
7. M.D. Sokoloff et al., Phys Rev Lett. **57**, 3003 (1986);
- 9a. R. Yoshida, Ph.D. Thesis, Northwestern University (1990) unpublished;
- 9b. H. Mendez, Ph.D. Thesis, Univ. of Mexico (1990) unpublished;
- 9c. M. Giannarchia, Ph.D. Thesis, Univ. of Milano (1990) unpublished;
- 9d. P. Vitulo, Thesis, Univ. of Pavia (1990) unpublished;
- 10a. R. Brun et al., "Geant 3", CERN Data Handling Div. DD/EE/84-1;
- 10b. P. Le Brun, S. Culy, C. Castoldi, "A guide to the Geant based User Code for the E687 Spectrometer" E687 internal note;
11. H. Friischi, Phys Lett. **67B**, 217 (1977);
- 12a. E. Eichten et al., Rev Mod Phys. **56**, 576 (1984);
- 12b. F. Bergsma et al., Phys Lett. **123B**, 257 (1983).

Figure Captions

- Fig. 1 Sketches of VDM (fig. 1a) and PGF (fig. 1b) Model's diagrams.
- Fig. 2 Sketch of the E687 experimental setup and apparatus (for more detailed explanations see: FNAL Report FN-553)
- fig. 3 Dimuon mass distribution for the selected events having $M_{\mu\mu} > 1.0$ GeV.
- Fig. 4a Distribution of the difference $\Delta E = E_T - E_{T\gamma}$ for the candidate events; a cut $\pm 3\sigma$ have been applied to select elastic events.
- Fig. 4b Mass dimuon distribution for the selected elastic events.
- Fig. 5 $dN/d(-t)$ distribution for all energies.
- Fig. 6a Comparison of the photon energy spectrum generated by using Bethe-Heitler normalization (dot points) and BGM normalization (full histogram). The low energy region (not used) is shown for sake of completeness.
- Fig. 6b MonteCarlo generated spectrum of the Wide Band Photon Beam.

- Fig. 7** Comparison of the acceptances for Bethe Heitler events (dashed histogram) and J/ ψ dimuon events (full histogram).
- Fig. 8a** Comparison of the cross sections measured with the two methods (only for sake of presentation, the data points are shifted in energy by ± 5 GeV).
- Fig. 8b** Compilation of the world existing data on J/ ψ photoproduction. The curves represent the prediction of two PGF models assuming $m_c=1.5$ GeV; the solid curve is formulae (5) to (7); the dotted curve is the PGF Model using the gluon distribution of ref. 12a.
- Fig. 8c** Same as fig. 8b in log scale. The curves are PGF predictions. Solid line: same as fig. 8b; dashed line: formula (8) instead of (6) and $m_c=1.5$ GeV; dashed-dotted line: formula (8) instead of (6) and $m_c=1.6$ GeV.

DISCLAIMER

This report was prepared as an account of work sponsored by an agency of the United States Government. Neither the United States Government nor any agency thereof, nor any of their employees, makes any warranty, express or implied, or assumes any legal liability or responsibility for the accuracy, completeness, or usefulness of any information, apparatus, product, or process disclosed, or represents that its use would not infringe privately owned rights. Reference herein to any specific commercial product, process, or service by trade name, trademark, manufacturer, or otherwise does not necessarily constitute or imply its endorsement, recommendation, or favoring by the United States Government or any agency thereof. The views and opinions of authors expressed herein do not necessarily state or reflect those of the United States Government or any agency thereof.

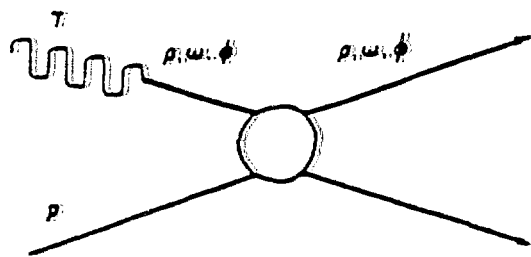


Fig. 1a

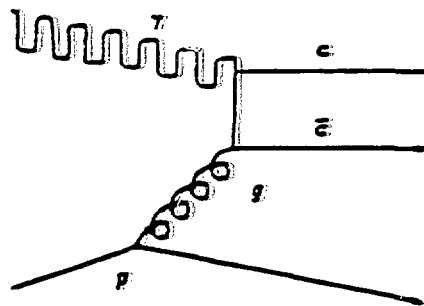


Fig. 1b

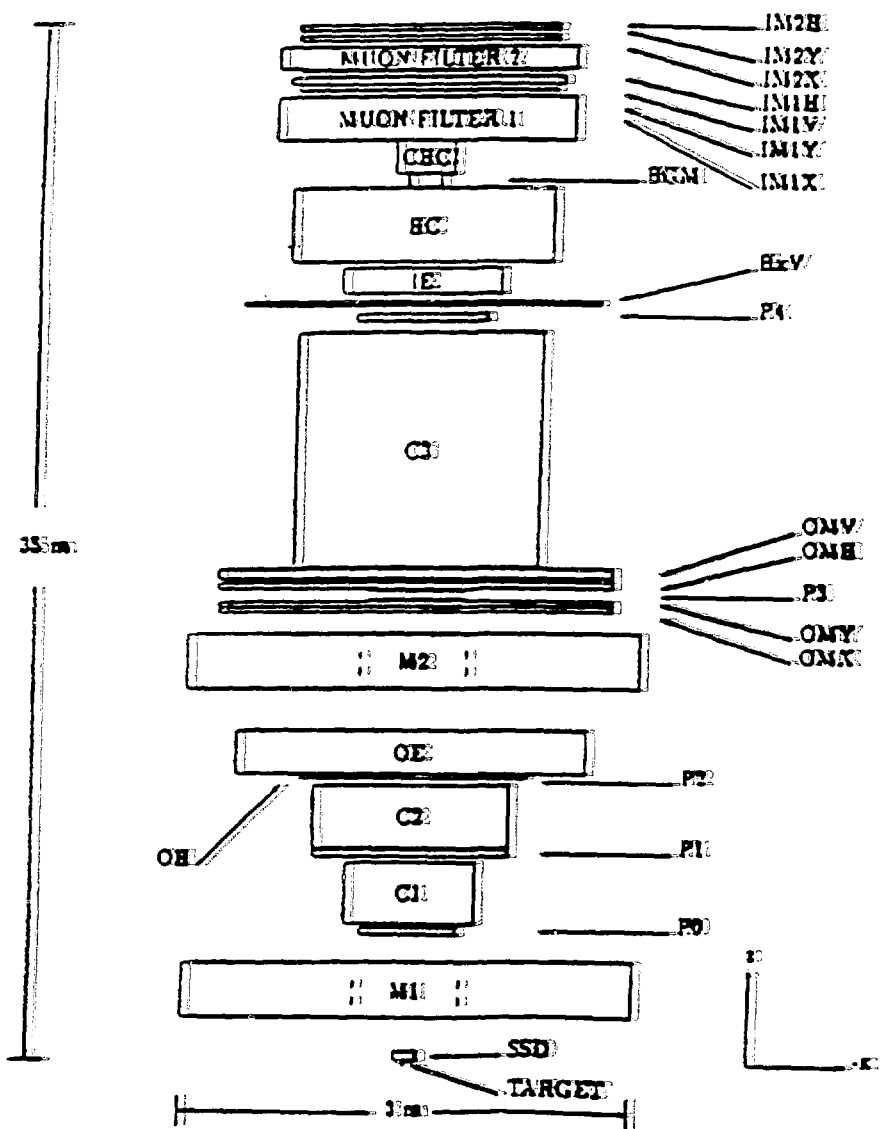


Fig. 2

$\mu^+ \mu^-$ INVARIANT MASS

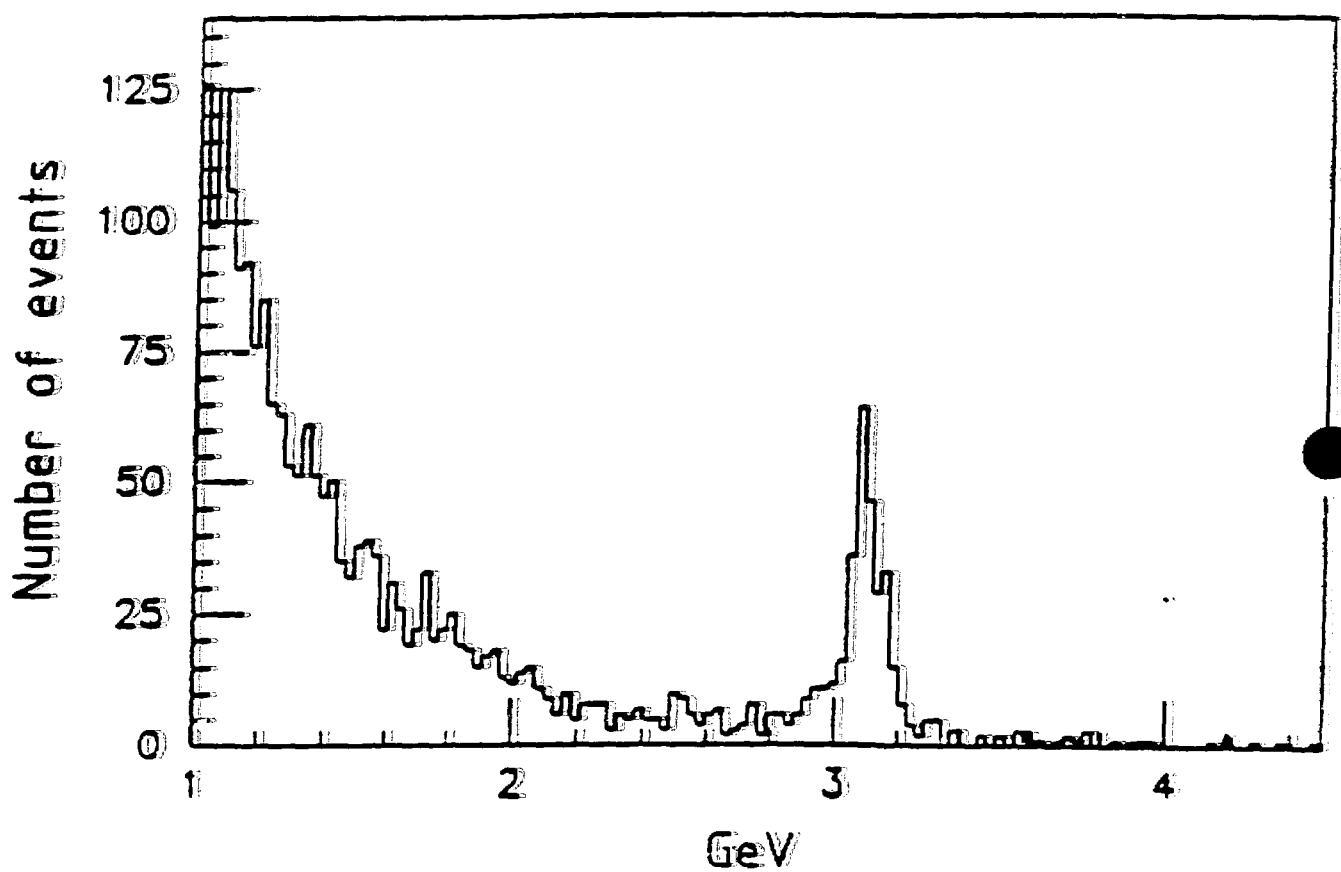


Fig. 3

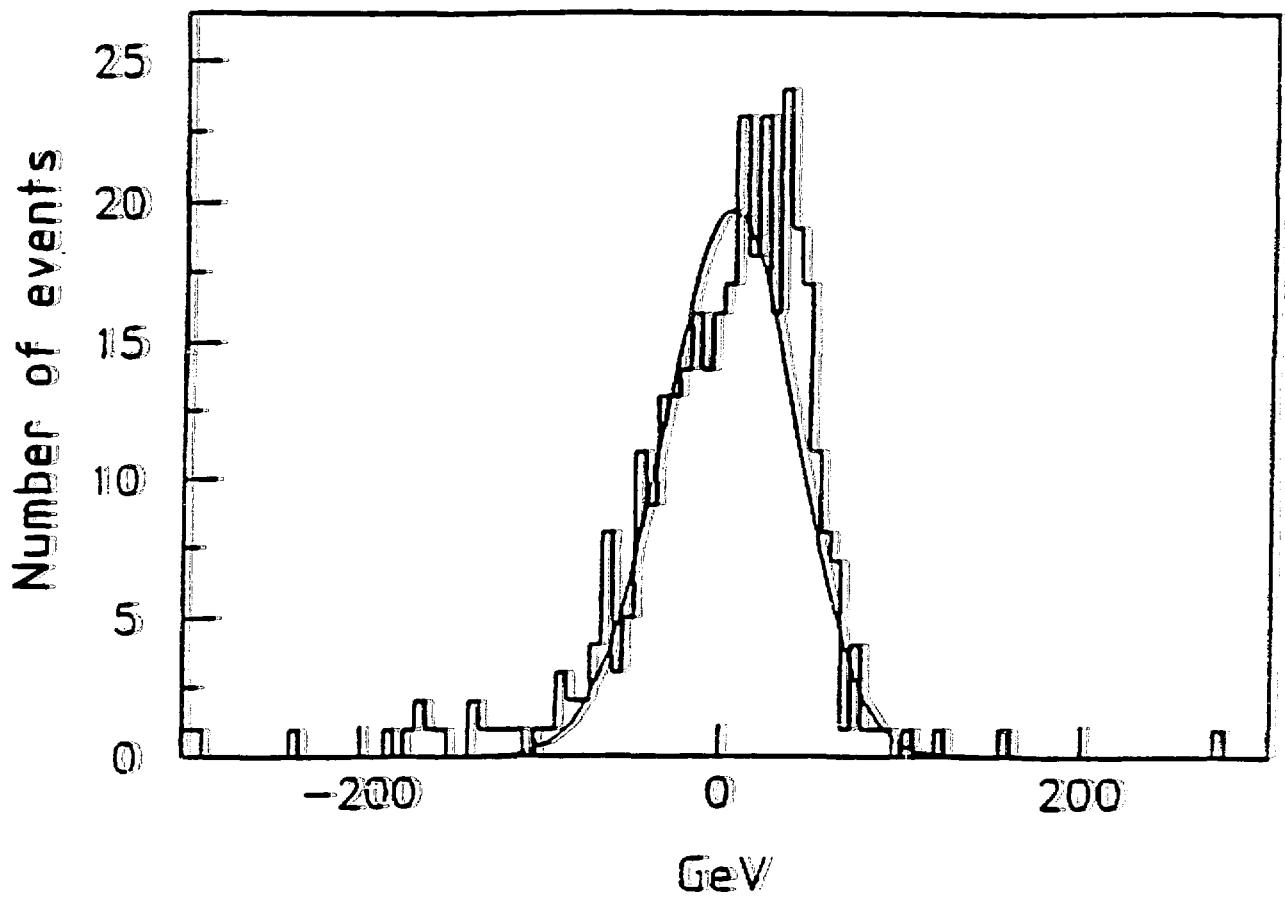


Fig. 4a

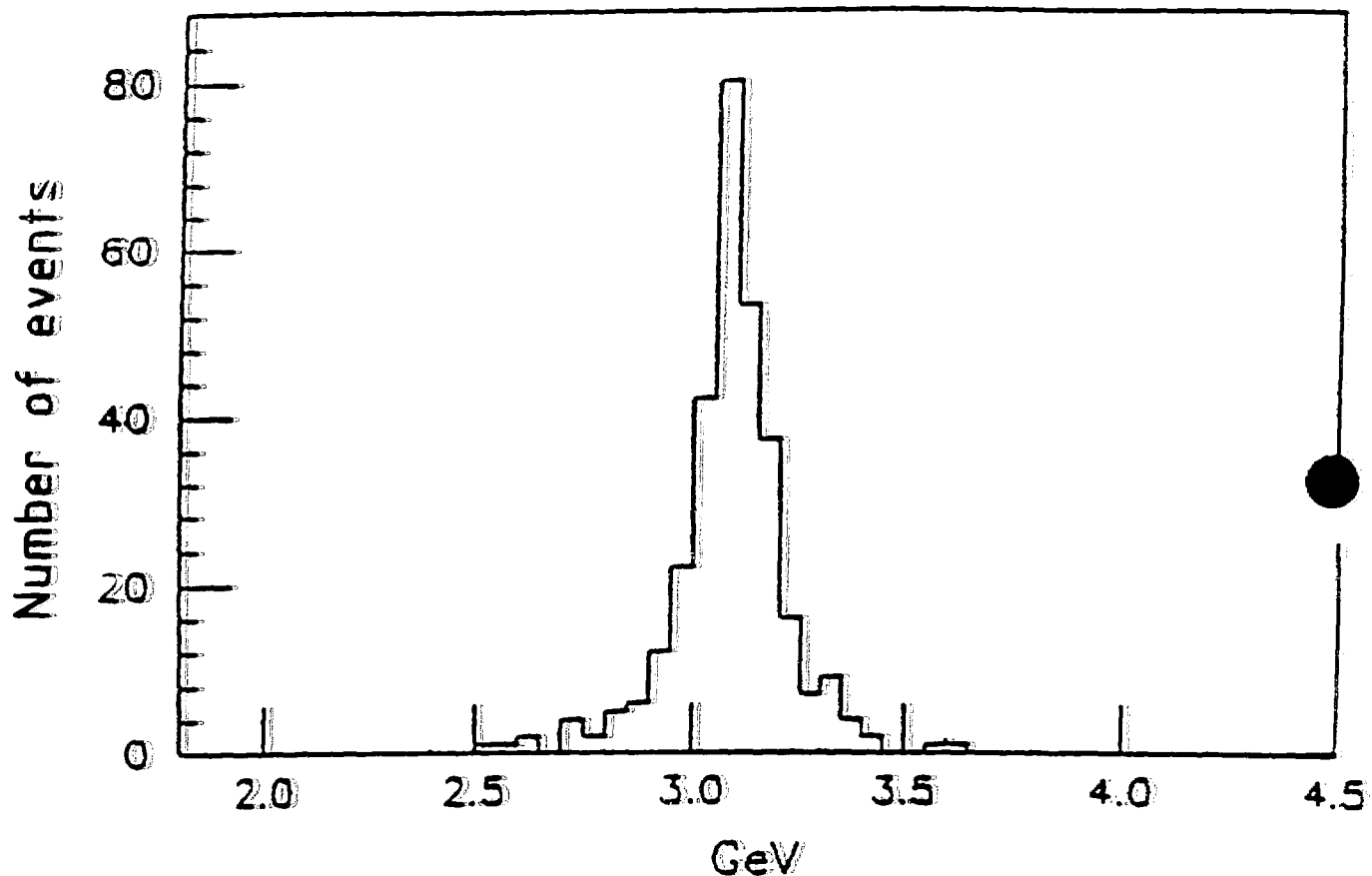


Fig. 4b

EVENTS / GEV $\star\star$ 2

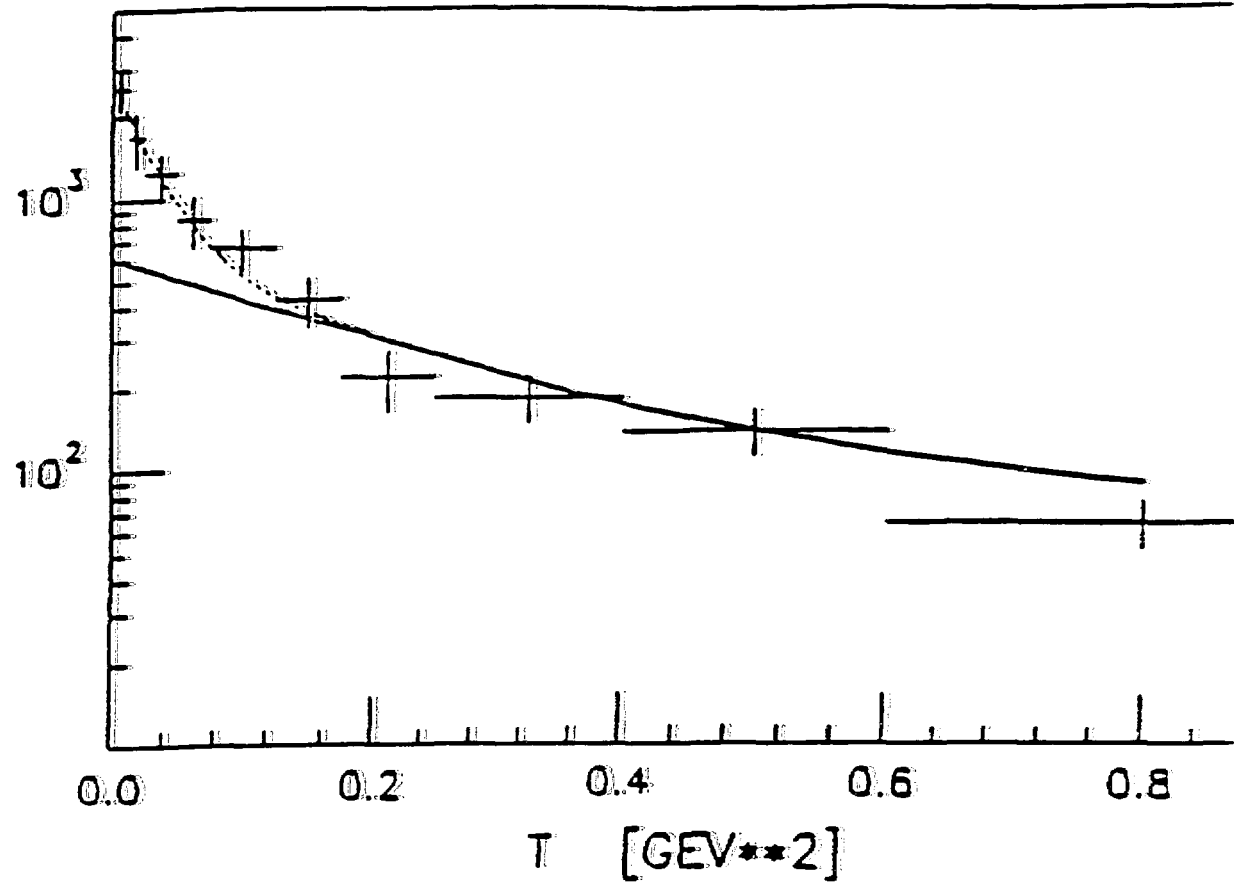


Fig. 5

PHOTON FLUX

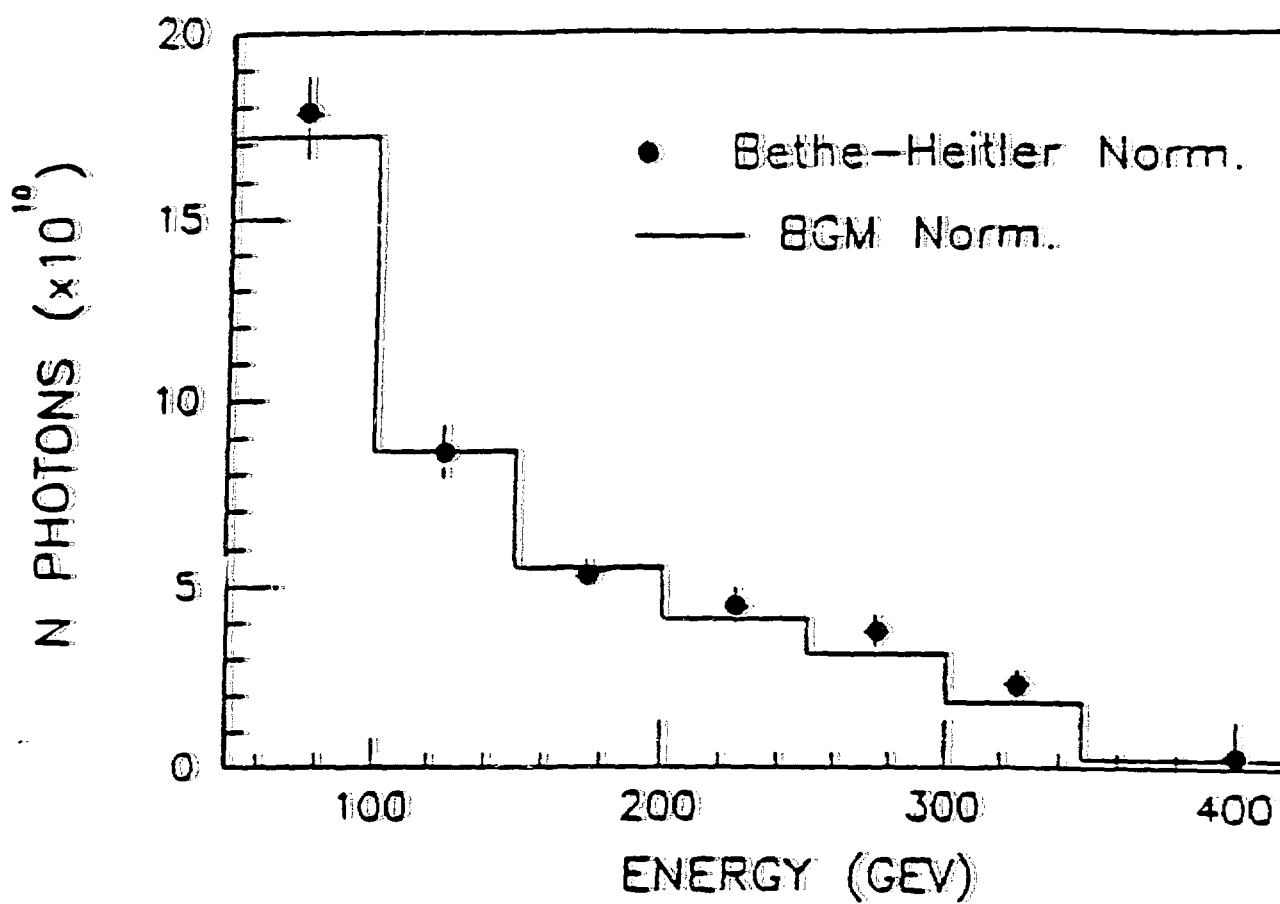


Fig. 6a

NUMBER OF PHOTONS (ARE: SCALE)

PHOTON SPECTRUM

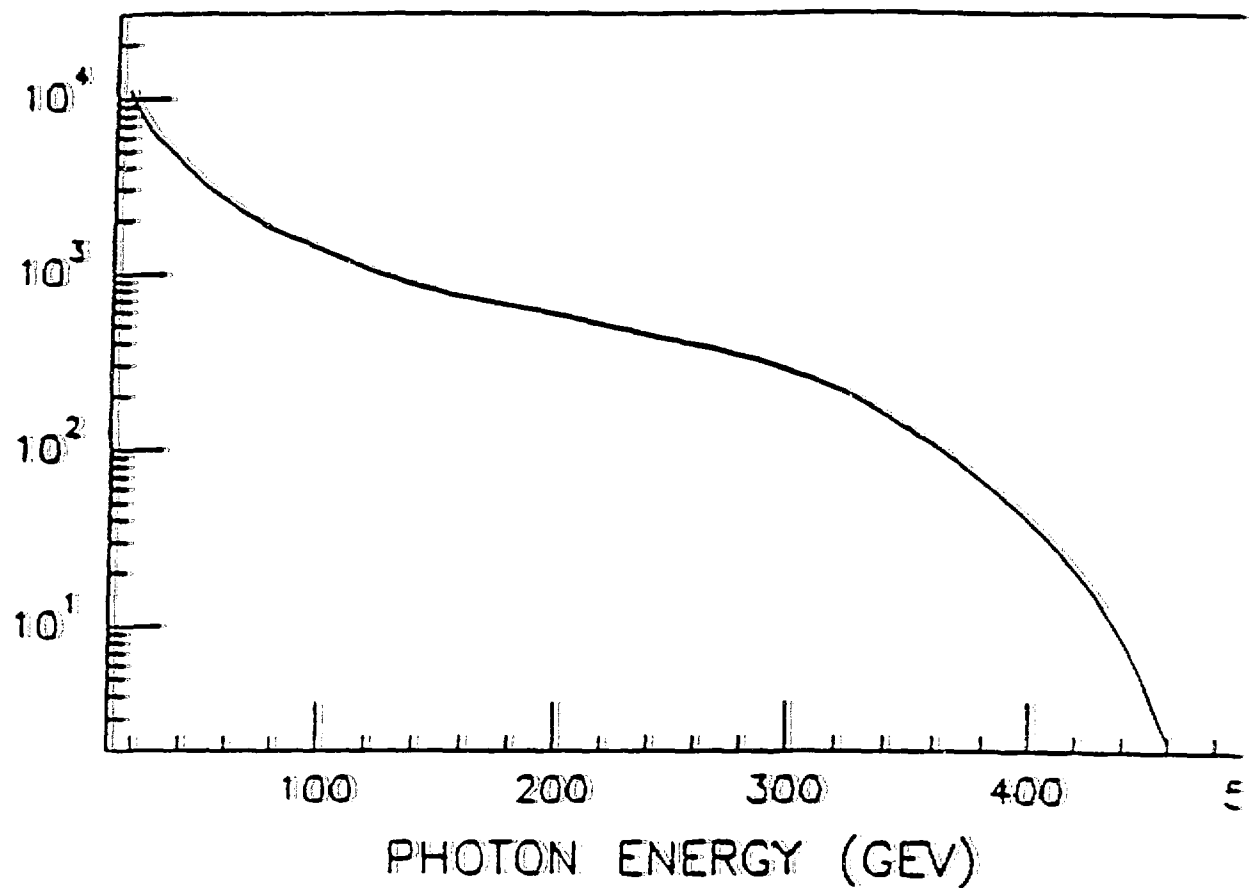


Fig. 6b

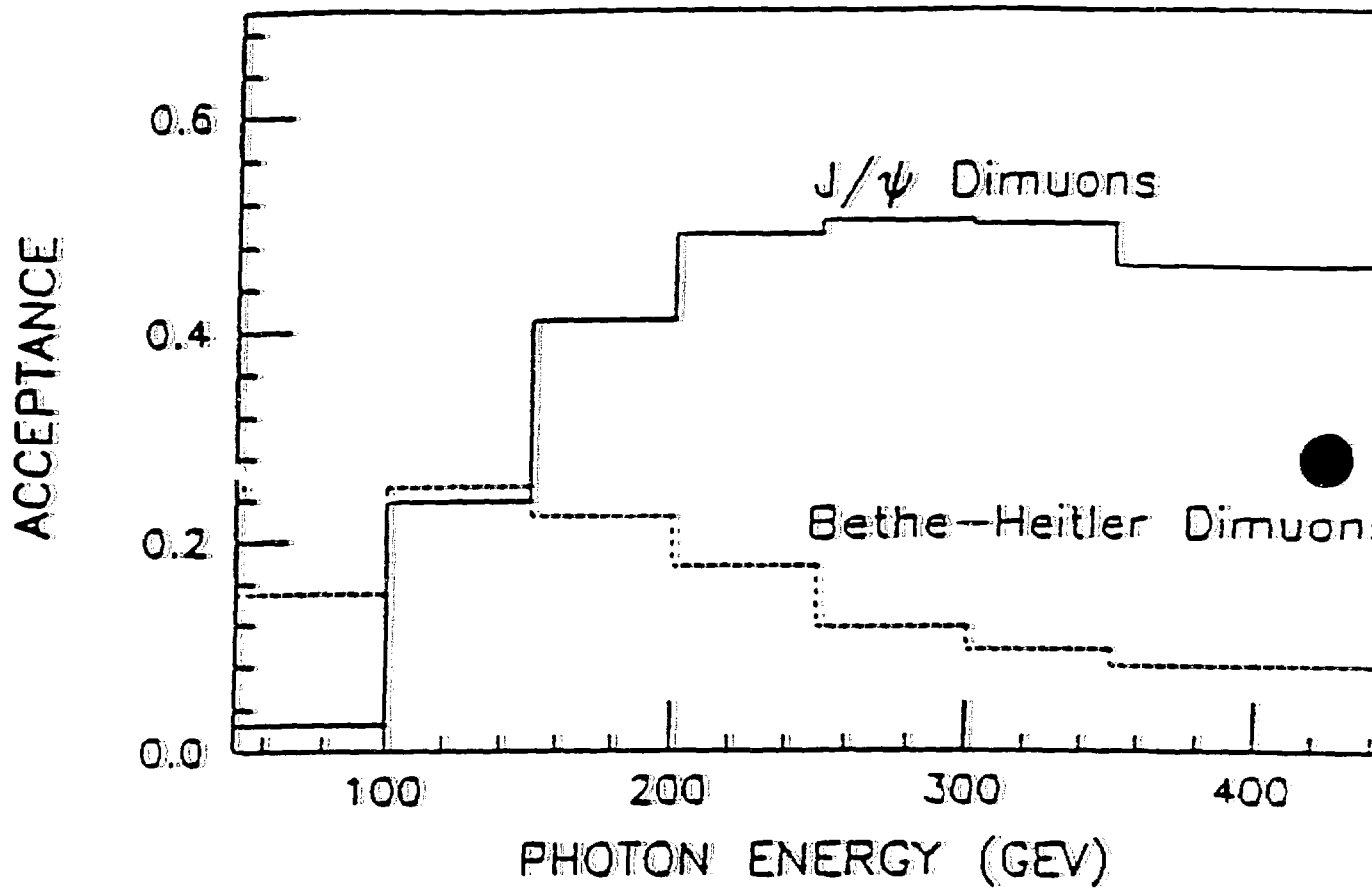


Fig. 7

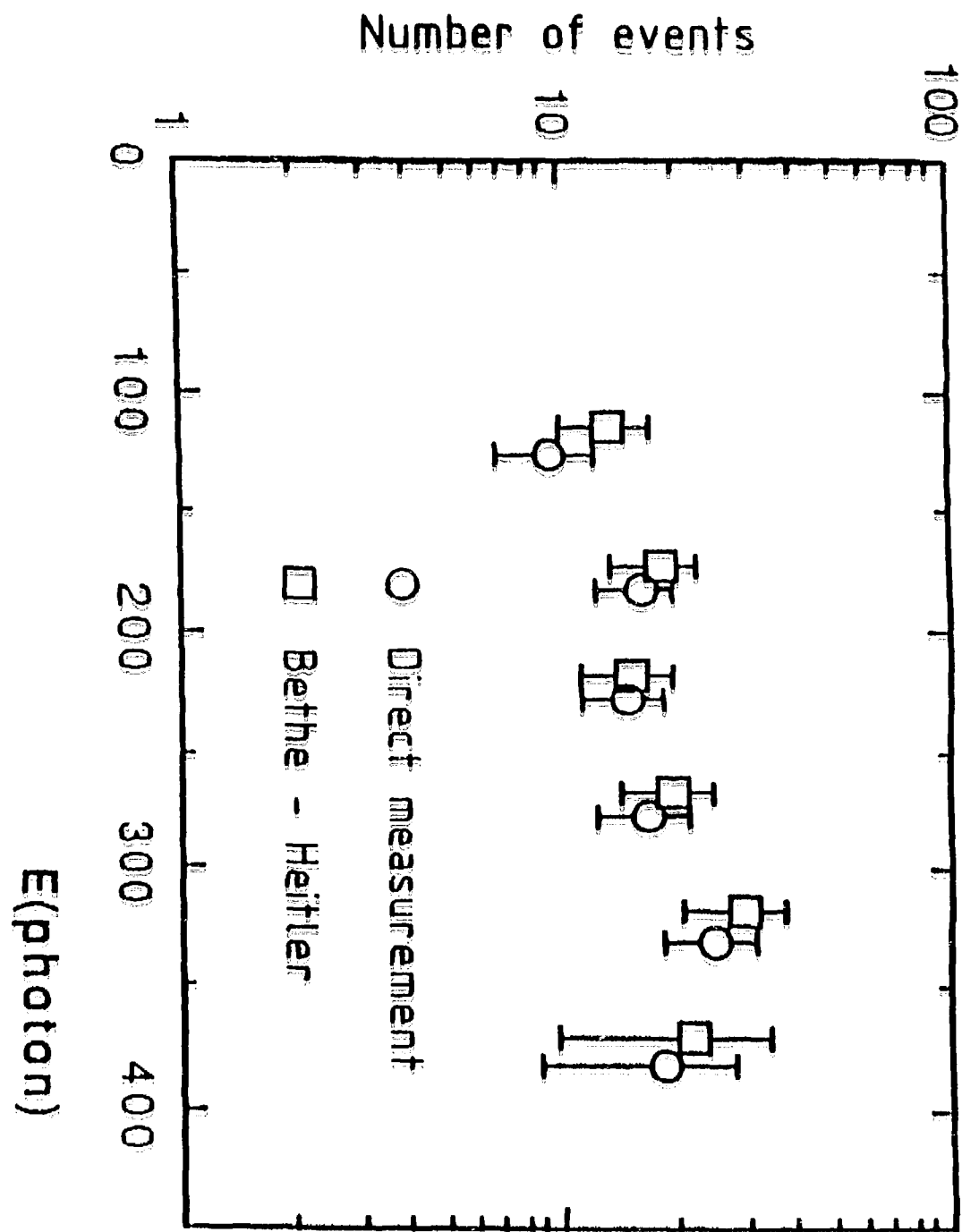


Fig. 8a

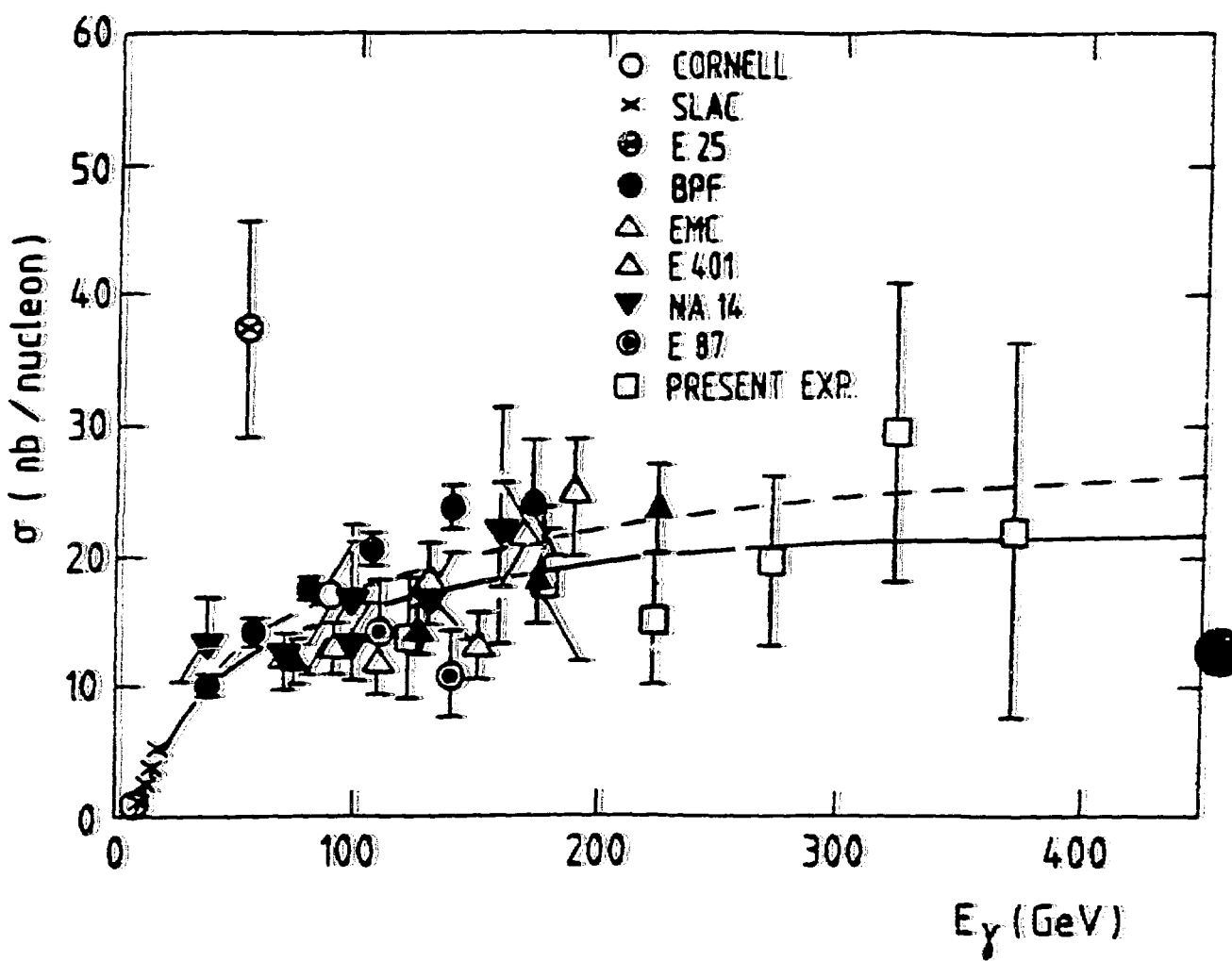


Fig. 8b

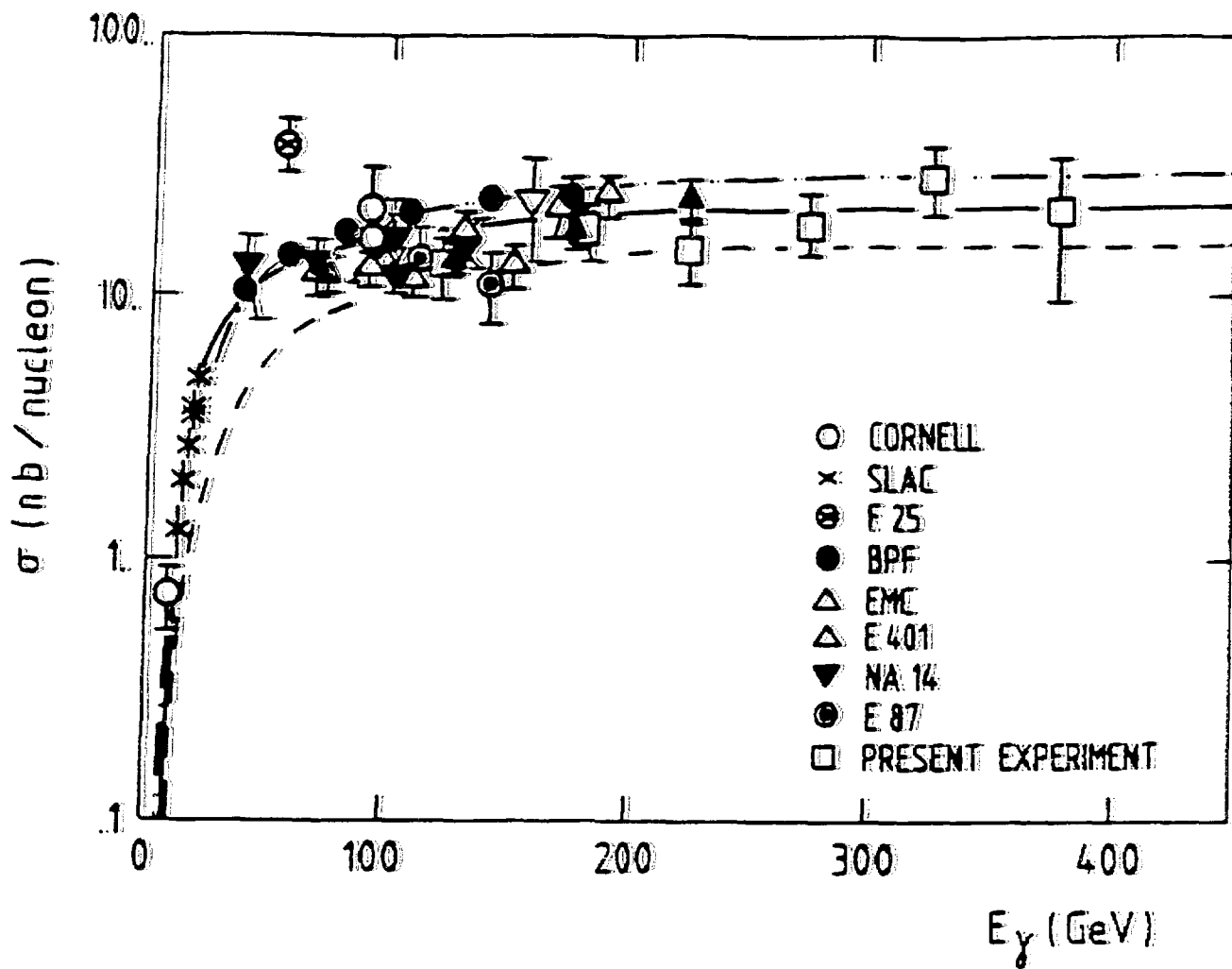


Fig. 8c